Opto-Electronic Advances

Supplementary information

August 2023, Vol. 6, No. 8

DOI: 10.29026/oea.2023.220141

Planar peristrophic multiplexing metasurfaces

Jia Chen[1,2], Dapeng Wang[1,2]*, Guangyuan Si[3], Siew Lang Teo[4], Qian Wang[4]* and Jiao Lin[5]*

[1]School of Electronic Science and Engineering (National Model Microelectronics College), Xiamen University, Xiamen 361005, China; [2]Innovation Laboratory for Sciences and Technologies of Energy Materials of Fujian Province (IKKEM), Xiamen 361005, China; [3]Melbourne Centre for Nanofabrication, Victorian Node of the Australian National Fabrication Facility, Clayton 3168, VIC, Australia; [4]Institute of Materials Research and Engineering, Agency for Science, Technology, and Research (A*STAR) 2 Fusionopolis Way, Innovis 08-03, Singapore 138632, Singapore; [5]School of Engineering, RMIT University, Melbourne, Victoria 3001, Australia.

*Correspondence: DP Wang, Email: dapengwang077@gmail.com; Q Wang, E-mail: wangqian@imre.a-star.edu.sg;
J Lin, E-mail: joe.lin@ieee.org

This file includes:

Supplementary information for this paper is available at https://doi.org/10.29026/oea.2023.220141

Section 1: Principle of the detour phase in the meta-hologram

The principle of the detour phase in the meta-hologram is shown in Fig. S1. Considering a monochromatic plane wave impinging on a metasurface with an identical periodicity and structural size, the phase retardation of diffraction light between any two adjacent nanostructures is expressed as

$$\Delta\phi = 2\pi a\sin(\theta)/\lambda \ , \tag{S1}$$

where a is the distance between adjacent unit cells; λ is the incident wavelength; θ is the diffraction angle.

The wavefront would not be modulated when the distance between two adjacent nanostructures is locally identical. As a result, by varying the distance a, we can obtain variety of 0–2π phase distributions. Furthermore, these isotropic nanostructures can be extended to a two-dimensional periodic array and choose the period length a. An interface seen by an observer standing at an angle θ from the normal can be discretized by sections of two perpendicular directions width a, each of which can then be apertured to select a phase within the 2π range by adjusting the plasma circular pore position in each period. To form a hologram with two-dimensional phase distribution $\phi_{(x,y)}$, the nanostructure position shift of the plasma circular pore to the center of its period $\delta_{(x,y)}$ in each unit cell is determined

$$\delta_{(x,y)} = \lambda \cdot \phi_{(x,y)} \Big/ 2\pi\sin(\theta) \ . \tag{S2}$$

Finally, the desired phase distribution is obtained by a two-dimensional array with different location shifts $\delta_{(x,y)}$. The generated holographic pattern is received at the diffraction angle θ

$$\theta = \arcsin(\lambda/\delta_{(x,y)} - \sin(\theta_0)) \ , \tag{S3}$$

where θ_0 is the oblique incidence angle. In general, detour-phase holograms are composed of many scatters (pixels) and each one is viable to realize a desirable phase delay. Thus, a metasurface is formed by a series of dislocated nanostructures to achieve the true phase-modulated holography.

In our case, the isotropic nanostructures as a kind of basic and undecorated building blocks are studied for purely validating the spatial frequency orthogonality as a new degree of freedom. According to the Babinet's principle[S1,S2], nanoholes and nanodisks of known size and shape can be regarded as a pair of complementary building blocks. The diffraction patterns from complementary apertures and opaque bodies are quite similar except for the forward scattering intensity. In addition to the trade off between the ease of nanofabrication and diffraction efficiency, the reflective configuration is accordingly adopted.

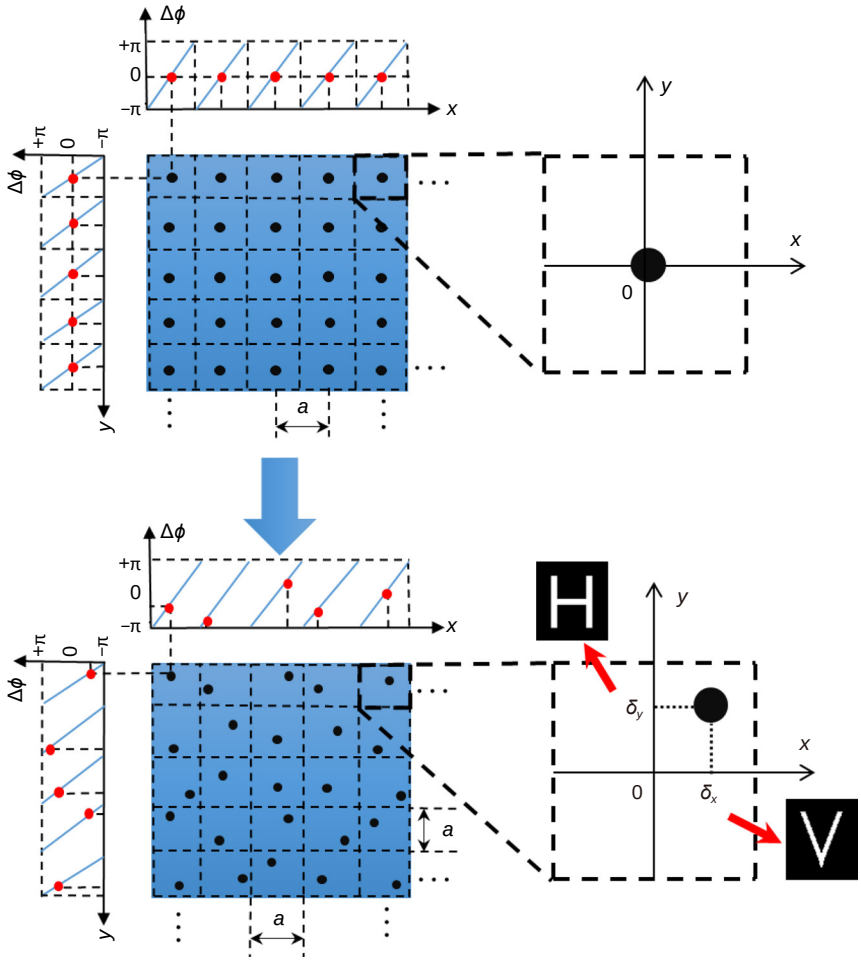

Fig. S1 | The conceptual scheme of subwavelength detour phase. The principle is to use the relative position of a transparent nanohole to achieve an arbitrary phase modulation. When a monochromatic plane wave is incident on an array of dislocated nanoholes, there is an additional phase $\Delta\phi$ of adjacent diffracted light waves and the range is $-\pi$~$+\pi$. Multiplexed holography can be achieved by using this subwavelength detour phase principle with different spatial frequency conditions.

Section 2: Effect of gold film thickness and pore size on transmittance

In order to optimize the structural parameters of the metasurface, we investigated the effect of the thickness of the gold film and the radius of the metal aperture on the transmittance. Figure S2 and Fig. S3 show the variation of the reflectance and transmittance in the wavelength range of 400–1100 nm for different thicknesses and apertures of the gold film. After analyzing the above results, the gold film with a thickness of h=200 nm and nanoholes with a radius of r=75 nm were selected for subsequent nanofabrication

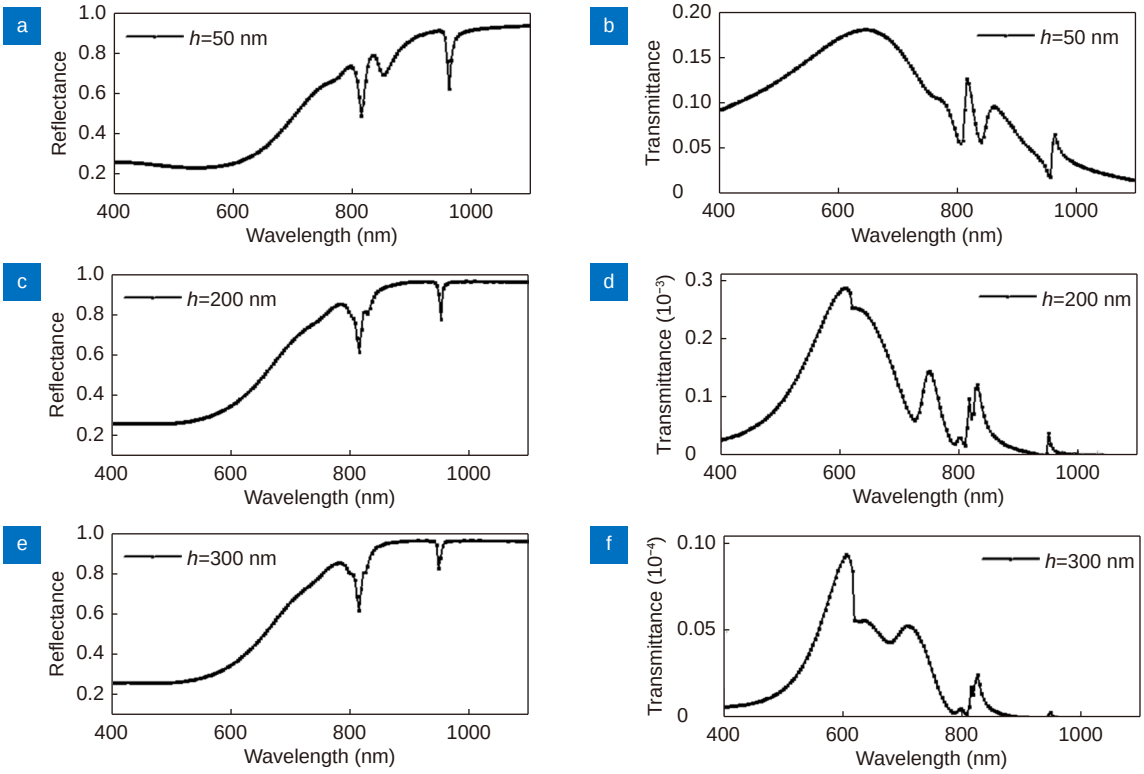

Fig. S2 | (**a**–**f**) The FDTD calculated the reflectance(a, c, e) and transmittance(b, d, f) using a single building block with the periodic boundary condition. The radius of nanoholes is fixed at 50 nm. The gold film thicknesses are varied with *h*=50 nm, *h*=200 nm, *h*=300 nm respectively and the wavelength range is 400–1100 nm.

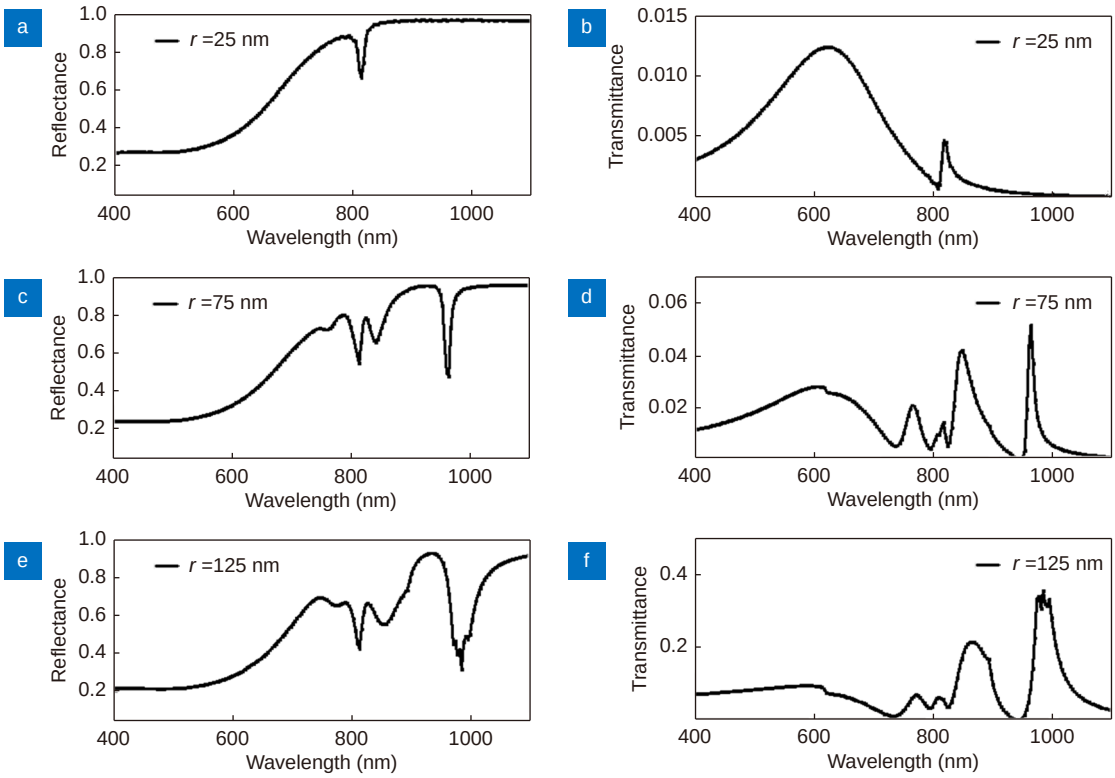

Fig. S3 | (**a**–**f**) The FDTD calculated the reflectance(a, c, e) and transmittance(b, d, f) using a single building block with the periodic boundary condition. The thickness of the gold film is fixed at 100 nm.The radius of nanoholes are varied (*r*=25 nm, *r*=75 nm, and *r*=125 nm) and the wavelength range is 400–1100 nm.

Section 3: Fabrication process of peristrophic multiplexing metasurface

Quartz substrates (n=1.46) were first cleaned by acetone and isopropyl alcohol and then rinsed by deionized water. After blow-drying with nitrogen, the substrates were put into an electron beam evaporator chamber (The Nanochrome™ II) for 200 nm gold deposition with 10 nm chromium as adhesion. Finally, metasurfaces were patterned by directly focused ion beam milling (FEI Helios Nanolab 600 FIB-SEM) using a 9.7 pA beam (gallium ions) current with 30 kV accelerating voltage.

Section 4: Convergence analysis of RMSE with different phase discrete levels

The required phase profile for "H" and "V" have been calculated based on Gerchberg–Saxton algorithm. As the number of iterations rises under the constraint of various discretized phase levels, the RMSE (Root Mean Square Error) function is introduced to monitor the quality of the resulting reconstruction image of the hologram. When the number of iterations is low, the RMSE between the initial and the retrieving image is relatively great. The reconstruction would exhibit a quick convergence and a stable trend as the number of iterations rises.

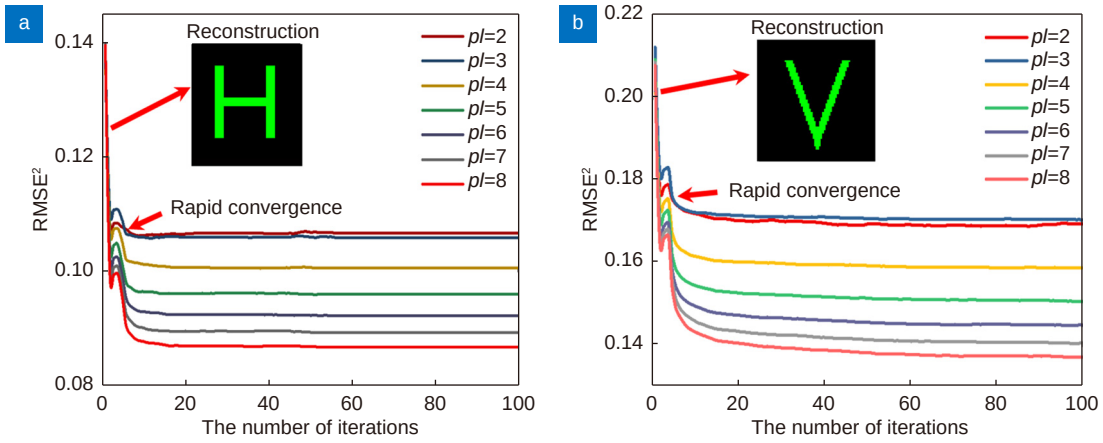

Fig. S4 | (**a**, **b**) The variation of root mean square error results (RMSE) of the reconstructed image "H", "V" with different discretized phase levels (*pl*=2, *pl*=3, *pl*=4, *pl*=5, *pl*=6, *pl*=7, *pl*=8), respectively. The RMSE of the reconstructed image shows a rapid convergence as the number of iterations increases.

Section 5: FDTD simulation results of transmitted and reflected of metasurface with different peristrophic angles

The principle of peristrophic multiplexing can be explained that when the incident beam is a plane wave with a special spatial frequency, the distinguishing playback of holograms is attainable through the relative rotation around an axis normal to the sample. As shown in Fig. S5, different images are reconstructed by the off-axis observation taking place in the transmitted and reflected domains, whilst the metasurface is rotated around the rotation axes 1 and 2. Theoretically, the multiplexing metadevice has the ability to exhibit distinguishing holograms in both transmitted and reflected fields. Hence, the holographic results in two cases are exhibited by means of finite-difference time-domain (FDTD) simulation. Noteworthy that, the position of the incident light at the initial position is set to remain coincident with the rotation axis 1. And the θ_1 and θ_2 indicate the rotation angle of the metasurface around the axis 1 and 2, respectively. Specifically, in the case where the incident spatial frequency light $k_{\text{wave}} = 1.18 \times 10^{-2}\ \text{nm}^{-1}$ is kept constant, and $k_{\text{s}} = 1.25 \times 10^{-2}\ \text{nm}^{-1}$. Besides the calculation based on the Fourier transform, the simulated results during the corresponding rotation can be done by the full-wave FDTD method. For the qualitative verification, the simulations of a low resolution (50*50 pixels) level were carried out.

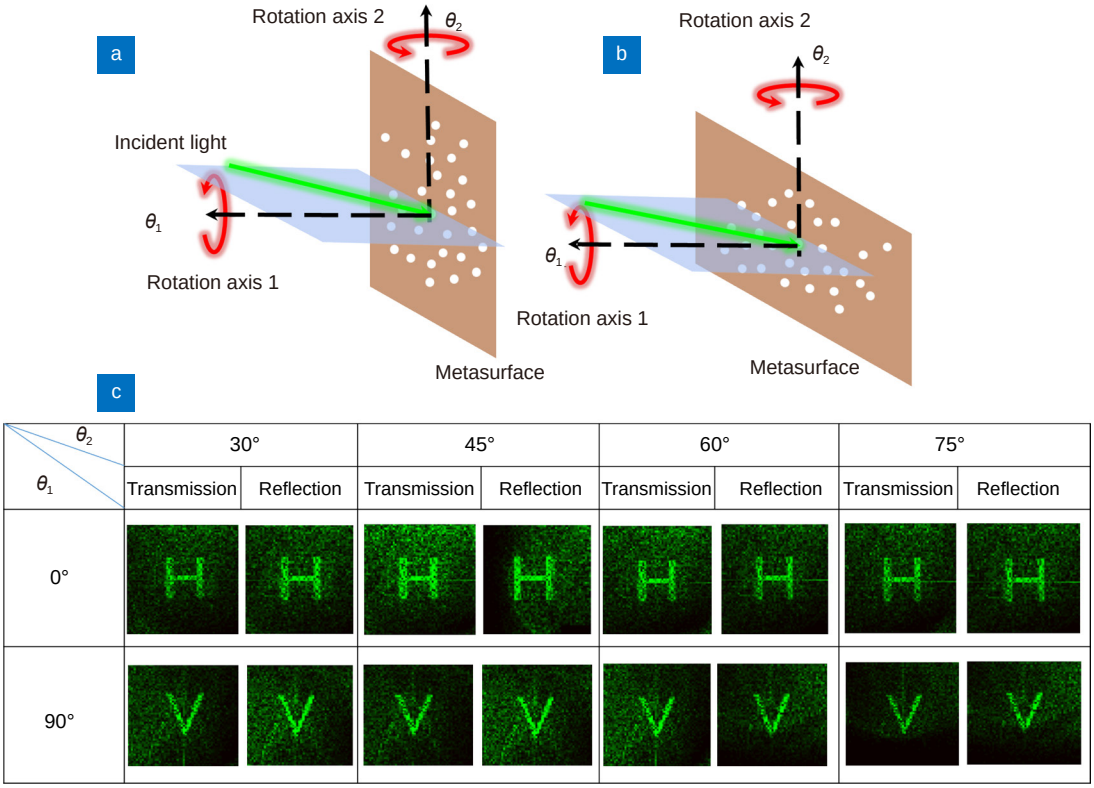

Fig. S5 | (**a**, **b**) Schematic of multiplexing the metasurface by rotating around axis 1. (**c**) FDTD simulation results of the meta-hologram in transmission and reflection directions during rotation around the axis 1 (0°, 90°) and the axis 2 (30°, 45°, 60°, 75°).

Section 6: Experimental and simulation results of multiplexing 0 and 1 images

Another multiplexed holograms (0 and 1 images, 200*200 pixels) were experimentally realized to exhibit the targeted information reconstruction. Both theoretical and experimental results are verified accordingly.

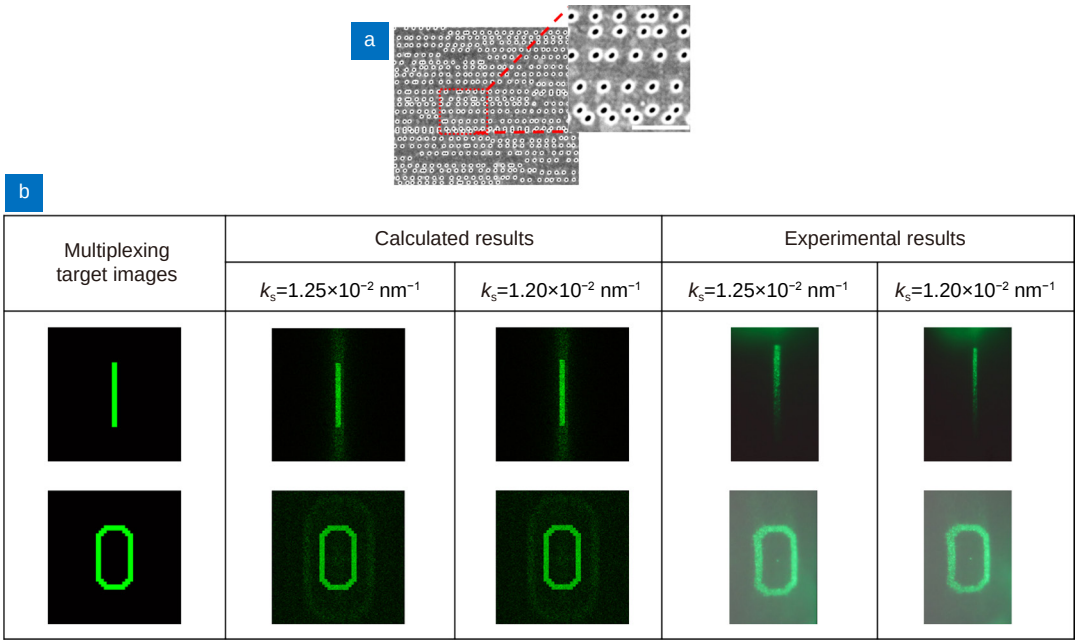

Fig. S6 | (**a**) Top-view SEM images of a multiplexing meta-hologram with two channels. The inserted scale bar is 1 μm. The meta-hologram is 200*200 pixels. The diameter of nanoholes is ~150 nm. (**b**) The initial, simulated and experimental "0" and "1" holographic results when the metasurface is rotated around the axis normal to the sample in different k_s.

Section 7: Multiple-channel multiplexing using a synthetic peristrophic meta-hologram

By adopting our method, a four-channel multiplexing metasurface in which all the information is highly integrated and encodes to the peristrophic angles of 0°, 45°, 90°, and 135° can be also realized. We combined the two-channel H/V and two-channel 0/1 multiplexing metasurfaces. The specific implementation process is shown in Fig. S7(a). The phase encoding of two pairs of target images H/V and 0/1 is done in two mutually perpendicular directions using the principle of detour phase encoding. Note that all the channels (Metasurface 1 and Metasurface 2) of the meta-holograms can be generated independently. Keeping the Metasurface 1 fixed, the Metasurface 2 is superimposed onto the Metasurface 1 after rotating through 45 degrees to create a new synthetic multiplexed metasurface. The schematic of the synthetic metasurface structure for quadruplexing is demonstrated in Fig. S7(b). In particular, the incident light maintains constant, the rotation angle θ_2 to the axis 2 is fixed at 45°, the rotation angle θ_1 to the axis 1 is 0°, 45°, 90°, 135° in the clockwise direction, and the reconstruction of "1", "H", "0", and "V" images can be observed in turns (Fig. S7(c)). Additionally, Fig. S7(d) displays the simulation results by means of FDTD solution, which is in line with the outcomes of the anticipated design.

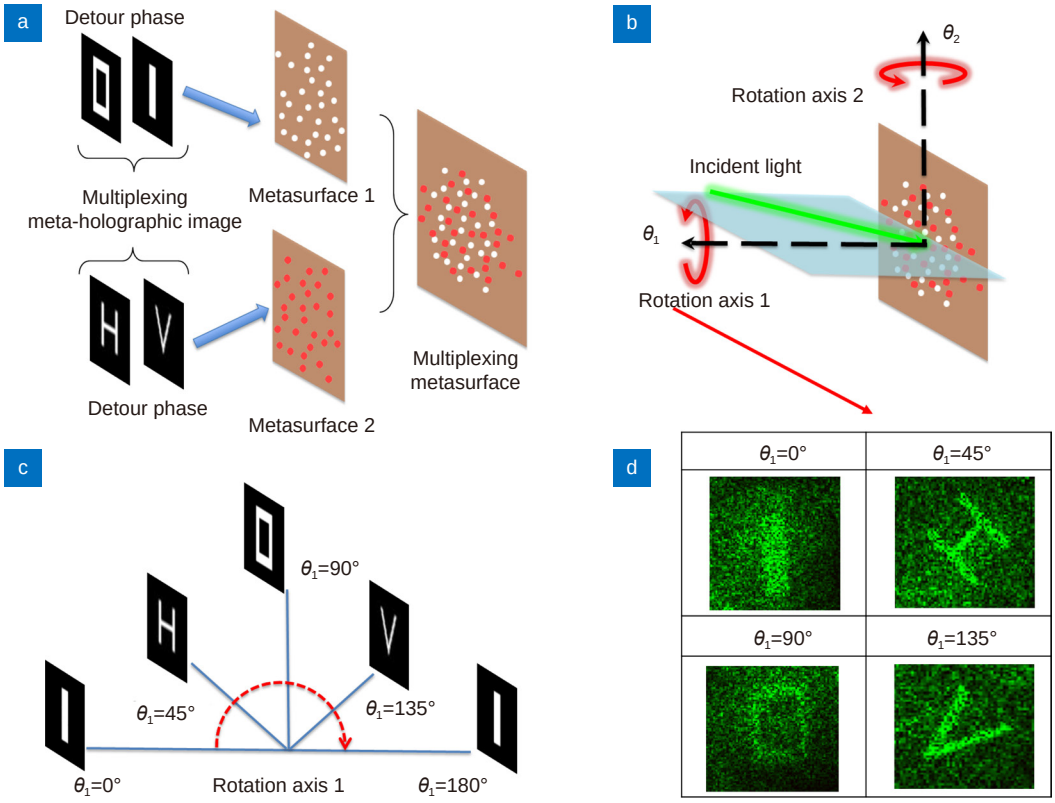

Fig. S7 | (**a**) Schematic quadruplexing of the synthetic metasurface. (**b**) The proof-of-concept for quadruple channel multiplexing. (**c**) The peristrophic reconstruction of "1", "H", "0", and "V" patterns by rotating the synthetic metasurface around the 1 axis (0°, 45°, 90° and 135°, respectively). (**d**) FDTD simulation results of the quadruple meta-holograms.

It should be noted that as the number of rotational multiplexing channels increases, the signal-to-noise ratio and isolation of the reconstructed target information of each channel will decrease significantly. This is primarily ascribed to the overlap or gap effect of adjacent building blocks during the stacking process. Reducing the crosstalk and enhancing the signal-to-noise ratio for peristrophic multiplexing metasurface would overcome in future. It is worth mentioning that, for the peristrophic multiplexing by the spatial frequency orthogonality, the two-channel holograms represent an excellent reconstruction performance. With the increase of multiplexing channels, the crosstalk will be inevitably introduced. Fig. S7 shows the four-channel multiplexing results using a synthetic peristrophic meta-hologram with four rotation angles. For further improving the multiplexing dimensionality, the synthetic strategy should be exploited. By integrating the wavelength, phase, polarization or OAM degree of freedom into the multitasked metadevices[S3,S4], the high-dimensional multiplexing could be realized.

Section 8: Schematic diagram of the experimental setup of DE measurement

In order to verify the polarization-independent and the versatility of our designed meta-hologram, the experimental setup is schematically shown in Fig. S8. Though the detectable holograms can be experimentally observed at the +1st reflective diffraction order, the most of energies are consumed at the zero-order diffraction due to the absence of blazed phase gradient. In the experiment, the multiplexing holographic images are reconstructed by the off-axis observation taking place in the reflected field, whilst the metasurface is rotated around the rotation axes 1. And the experimental DE is evaluated by the ratio of the intensity of the reflected diffraction order carrying the target information (n = +1) to the total reflection power after the excitation of the rotational multiplexing metasurface.

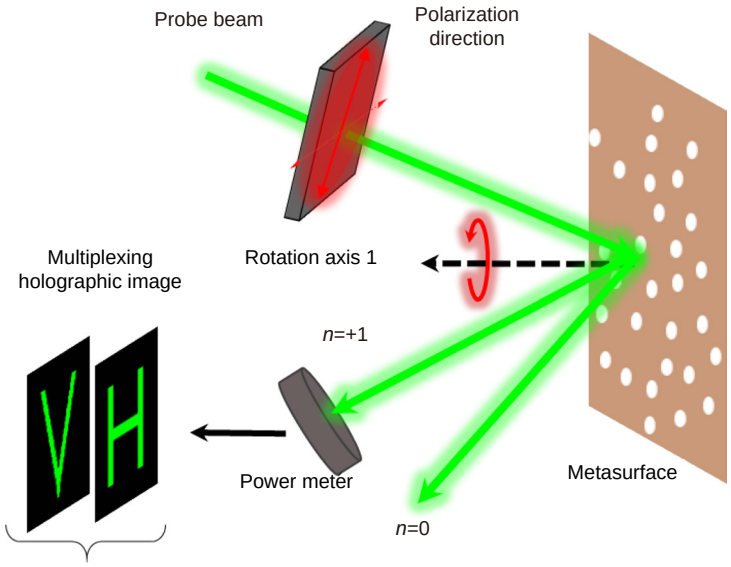

Fig. S8 | Schematic diagram of the experimental setup of DE measurement.

References

S1. Booker HG. Slot aerials and their relation to complementary wire aerials (Babinet's principle). *J Inst Electr Eng* **93**, 620–626 (1946).
S2. Falcone F, Lopetegi T, Laso MAG, Baena JD, Bonache J et al. Babinet principle applied to the design of metasurfaces and metamaterials. *Phys Rev Lett* **93**, 197401 (2004).
S3. Deng ZL, Deng JH, Zhuang X, Wang S, Li K et al. Diatomic metasurface for vectorial holography. *Nano Lett* **18**, 2885–2892 (2018).
S4. Ouyang X, Xu Y, Xian MC, Feng ZW, Zhu LW et al. Synthetic helical dichroism for six-dimensional optical orbital angular momentum multiplexing. *Nat Photonics* **15**, 901–907 (2021).